Dayside thermal structure of Venus' upper atmosphere characterized by a global model

A. S. Brecht[1] and S. W. Bougher[2]

[1] Observations of Venus' dayside thermal structure are being conducted through ground based observatories. These temperature measurements, along with those from several instruments onboard the current Venus Express mission, are augmenting the previous thermal structure data from past missions (e.g., Veneras', Pioneer Venus Orbiter, Pioneer Venus Probes). These recent ground-based and VEx observations reveal the Venus dayside lower thermosphere to be considerably warmer and dynamically important than previously understood. In this study, a three dimensional general circulation model, the Venus Thermospheric General Circulation Model (VTGCM), is used to provide dayside temperature predictions for comparison to these recent ground based observations. Such a comparison serves to identify and quantify the underlying thermal processes responsible for the observed dayside temperature structure. The VTGCM reproduces the dayside temperatures observed near 110 km at noon from 40°S to 40°N very well. In addition, the global winds generated by these warm dayside temperatures are shown to give rise to dayside upwelling (divergence) and nightside subsidence (convergence) resulting in nightside warming near the anti-solar point at ∼104 km. Corresponding nightside temperatures reach ∼198 K, in accord with averaged measurements. This agreement implies (1) it is important for GCMs to include the updated radiative heating and cooling rates presented in Roldán et al. (2000) and (2) the current VTS3 and VIRA empirical models are in-sufficient in representing the warm regions observed in the thermal structure of the dayside lower thermosphere (∼100 to 130 km) and need to be updated.

1. Introduction

[2] Continuous observations of Venus' dayside thermal structure are crucial in helping constrain atmospheric models (e.g., climatology, variability). Additionally, models can provide analysis and interpretation of observations, thereby investigating underlying thermal balances maintaining and driving variations in these temperatures.

[3] Past missions (e.g., Veneras', Pioneer Venus Orbiter, Pioneer Venus Probes) have observed the thermal structure of Venus' atmosphere in select locations and local times (LT). The dayside thermal structure from the cloud tops (∼70 km) to ∼100 km was observed by Pioneer Venus (PV) with three different techniques; (1) temperatures derived from in situ density measurements [*Seiff and Kirk*, 1982], (2) remote sensing, including PV Orbiter infrared radiometry [*Taylor et al.*, 1980] and PV Orbiter radio occultations

[*Kliore and Patel*, 1980], and (3) in situ measurements by the PV probes (Day probe [30°S at 06:46 LT] and Large probe [4.2°N at 07:38 LT]) [*Seiff and Kirk*, 1982]. Above 100 km, two techniques were used to gather temperature data. One utilized the orbiter atmospheric drag measurements, and monitored the decay of the orbiter's orbit [*Keating et al.*, 1979a, 1979b, 1980]. The second technique measured species number density using two neutral spectrometers: a) the PV Bus Neutral Mass Spectrometer (BNMS) which sampled at a single local Venus time (08:30 LT) [*von Zahn et al.*, 1979, 1980]; b) the PV Orbiter Neutral Mass Spectrometer (ONMS) which obtained data at all local solar times near 16°N and to the lowest altitude near ∼140 km [*Niemann et al.*, 1979, 1980]. More details on these observations are discussed in *Seiff* [1983].

[4] These past PV observations, including also Venera and Mariner data, have been incorporated into two empirical models, VTS3 [*Hedin et al.*, 1983] and the Venus International Reference Atmosphere (VIRA) [*Keating et al.*, 1985]. These empirical models calculate global temperature structure and global densities [*Seiff et al.*, 1985; *Keating et al.*, 1985], and are used as tools for the Venus atmospheric community. However, these empirical models are limited to observational coverage and solar maximum fluxes. As discussed previously, the most comprehensive measurements (PV-ONMS) are for

---

[1]NASA Ames Research Center, Moffett Field, California, USA.
[2]Department of Atmospheric, Oceanic, and Space Sciences, University of Michigan, Ann Arbor, Michigan, USA.

Corresponding author: A. S. Brecht, NASA Ames Research Center, MSC 245-3, Moffett Field, CA 94035, USA. (amanda.s.brecht@nasa.gov)

low latitudes and above 140 km. The observations for lower altitudes are diurnally averaged. Further, fields are symmetrically distributed cylindrically at higher latitudes and the hydrostatic equilibrium assumption is utilized to extrapolate below 140 km. Due to the assumptions and extrapolations employed, these empirical models only provide a first order approximation to a reference atmosphere.

[5] Currently, Venus Express (VEx), a European mission, is collecting new measurements focusing upon Venus' thermal structure. The instrument SPICAV (Spectroscopy for Investigation of Characteristics of the Atmosphere of Venus) has mainly made observations on the nightside for an altitude range of ∼90 to ∼140 km [*Bertaux et al.*, 2007]. The VeRa (Venus Express Radio Science) instrument observes in an altitude range of ∼50 to ∼90 km [*Pätzold et al.*, 2007]. More recently, SOIR (Solar Occultation in the Infrared) has produced temperature profiles mostly on the terminators in the altitude range of ∼100 km to ∼150 km [*Mahieux et al.*, 2010]. Last, the VIRTIS (Visible and Infra-Red Thermal Imaging Spectrometer) instrument is capable of providing information on the thermal structure and has begun creating temperature maps focused upon the nightside (∼65–∼80 km) [*López-Valverde et al.*, 2007; *Drossart et al.*, 2007; *Grassi et al.*, 2008; *Gilli et al.*, 2009; *Grassi et al.*, 2010]. The most recent observations by VEx have shown the empirical models (VTS3 and VIRA) to be incomplete and not representative of Venus' constantly changing atmosphere [e.g., *Bertaux et al.*, 2007; *Pätzold et al.*, 2007; *Drossart et al.*, 2007].

[6] However, ground based techniques have begun to collect dayside temperature data more continuously, with greater spatial and temporal coverage [e.g., *Clancy et al.*, 2003, 2008; *Sonnabend et al.*, 2010; *Clancy et al.*, 2012; *Sonnabend et al.*, 2012]. One technique utilizes heterodyne spectroscopy of CO_2 at mid-infrared wavelengths (measurement of the non-local thermodynamic equilibrium (NLTE) emission of CO_2 near 10 μm). It was first applied to the Venus upper atmosphere by *Betz et al.* [1976] and most recently utilized to derive temperatures by *Sonnabend et al.* [2008, 2010] and *Sonnabend et al.* [2012]. This technique involves the measurement of infrared CO_2 absorption and emission lines near 110 km in the Venus atmosphere; i.e., from the doppler broadened line-width temperatures can be derived. For *Sonnabend et al.* [2010], the telescope had a diffraction limited field of view of 1–3 arcseconds. Data were collected recently during three observational periods; March 20–22 2009, April 2–6 2009, and June 2–6 2009 [*Sonnabend et al.*, 2010]. The angular diameter of Venus varied for the three observing periods; 53–56 arcseconds (March/April) and 23–25 arcseconds (June). Venus was at inferior conjunction (March 27, 2009) after the March observations and before the April observations. The June observation was at maximum western elongation. These observations span a range in LT and latitude, and refer to a single level measurement near 110 km altitude. The altitude of the emitting region is determined by "the ratio of collision induced to the probability of spontaneous emission for the excited CO_2 molecules" [*Sonnabend et al.*, 2008]. Table 1 in *Sonnabend et al.* [2010] lists the temperature measurements made during these observational periods, and the time and the location of these measurements. The observed temperatures range from 160 K near the South Pole to ∼200 K near

the terminators, with the warmest temperatures near noon at the equator (∼240–250 K).

[7] Another ground based technique used to measure Venus' dayside temperature structure focuses upon sub-millimeter ^{12}CO (346 GHz) and ^{13}CO (330 GHz) line absorption measurements [e.g., *Clancy et al.*, 2003, 2008, 2012]. The sub-millimeter technique employs a diffraction limited beam resolution of 13.5–14.5 arcseconds and is also capable of mapping temperatures across the disk of Venus. Recently, *Clancy et al.* [2012] have compiled dayside disk averages (LT = 10:30 to 13:30) for two different observing periods; 2000 to 2002 and 2007 to 2009. The apparent Venus disk ranged between 10 and 13 arcseconds. These average dayside observations return temperature profiles over an altitude range of 76 km to 106 km. The temperatures range from ∼180 K to ∼200 K, dependent on altitude.

[8] Previously, most ground based observations have focused upon Venus' nightside due to the extreme temperatures observed by the SPICAV instrument [*Bertaux et al.*, 2007]. These temperature measurements, supply more constraints for the observed nightside warm region between 90 km and 100 km near the equator which the empirical models do not reproduce. At this time, near 95 km, the range of observed temperatures on the nightside is ∼160 K up to 240 K [e.g., *Connes et al.*, 1979; *Seiff and Kirk*, 1982; *Schofield and Taylor*, 1983; *Seiff et al.*, 1985; *Clancy and Muhleman*, 1991; *Crisp et al.*, 1996; *Clancy et al.*, 2003; *Ohtsuki et al.*, 2005; *Zasova et al.*, 2006; *Bertaux et al.*, 2007; *Rengel et al.*, 2008; *Clancy et al.*, 2008; *Bailey et al.*, 2008; *Sonnabend et al.*, 2008; *Clancy et al.*, 2012]. In comparison, simulations from a three-dimensional model have been utilized with these observations to provide insight into the possible source(s) of the warming on the nightside [*Brecht*, 2011; *Brecht et al.*, 2011]. The results showed the nightside warm region to be associated with the dayside 4.3-μm heating warm region (near 115 km) and the resulting day-to-night global circulation. The downwelling component of this circulation produces dynamical heating near midnight.

[9] In this study, simulations from the Venus Thermospheric General Circulation Model (VTGCM) [*Brecht et al.*, 2011, 2012] will be utilized to calculate dayside temperatures for comparison to recent ground-based observations. This exercise will investigate the underlying heat balances giving rise to the Venus thermospheric dayside thermal structure. Specifically, this study will facilitate the validation of the latest implementation of the updated heating and cooling rates from *Roldán et al.* [2000] within the VTGCM. Furthermore, the revised temperature structure being measured by the new dayside observations and their close reproduction by the corresponding VTGCM simulations both suggest shortcomings in existing empirical models that are typically used to characterize the Venus upper atmosphere.

2. Venus Thermospheric General Circulation Model

2.1. Model Description

[10] The VTGCM is a 3-D finite difference hydrodynamic model of the Venus upper atmosphere [e.g., *Bougher et al.*, 1988, 1990, 1997, 1999, 2002, 2008; *Bougher and Borucki*, 1994; *Zhang et al.*, 1996; *Brecht*, 2011; *Brecht*

et al., 2011, 2012] which is based on the National Center for Atmospheric Research (NCAR) terrestrial Thermospheric Ionosphere General Circulation Model (TIGCM). Briefly, the VTGCM solves the time-dependent primitive equations for the neutral upper atmosphere; temperature, neutral-ion densities, and three-component neutral winds. The model domain covers a 5° by 5° latitude-longitude grid, with 69 evenly spaced log-pressure levels in the vertical, extending from approximately ~70 to 300 km (~70 to 200 km) at local noon (midnight).

[11] Formulations for CO_2 15-μm cooling, wave drag, and eddy diffusion are parameterized within the VTGCM using standard aeronomical formulations. "Exact" (line-by-line radiative transfer model) CO_2 15-μm cooling rates for a given temperature and composition profile are taken from *Roldán et al.* [2000]; cooling rates for the simulated VTGCM temperatures and species abundances are calculated (from these "exact" rates) based upon a slight modification of a parameterization scheme utilized previously [e.g., *Bougher et al.*, 1986]. The corresponding O-CO_2 collisional relaxation rate adopted for typical benchmark VTGCM simulations is now 3×10^{-12} cm^3 s^{-1} at 300 K [*Bougher et al.*, 1999]. This value provides strong CO_2 15-μm cooling that is consistent with the use of EUV-UV heating efficiencies of ~20–22%, which are in agreement with detailed offline heating efficiency calculations of *Fox* [1988]. The near-IR heating term is incorporated using offline simulated look-up tables, updated recently using *Roldán et al.* [2000] rates. The most notable consequence from updating the new IR rates is the doubling of the 4.3-μm heating around 115 km on the dayside. Previous studies [*Brecht et al.*, 2011] constrained the 15-μm cooling rates in this region using the radiative equilibrium temperature (RET) profile in *Roldán et al.* [2000, Figure 13] for a solar zenith angle (SZA) of 0 degree. However, upon further review and discussion, the displayed RET profile is more representative of conditions closer to SZA ~ 16° (M. A. López-Valverde, private communication, 2011). Furthermore, 15-μm cooling rates below ~80 km have been modified according to those employed in the Lee et al. Venus GCM model [*Lee et al.*, 2007; *Lee and Richardson*, 2010; *Lee et al.*, 2011]. These changes imply a warmer atmosphere closer to SZA ~ 0°, and a corresponding revision of the parameterized scheme for CO_2 15-μm cooling within the VTGCM.

[12] Wave drag is prescribed as Rayleigh friction in order to mimic wave-drag effects on the mean flow. For more detail on the Rayleigh friction and gravity wave drag formulations see *Bougher et al.* [1988] and *Brecht et al.* [2011]. The eddy diffusion coefficient on the nightside is prescribed in the form $K = \frac{A}{\sqrt{n}}$ with units of cm^2 s^{-1} where n is the total number density and A is a constant [*von Zahn et al.*, 1979]. The nightside eddy diffusion has a prescribed maximum value of 1×10^7 cm^2 s^{-1} and the dayside has a constant value for the entire upper atmosphere of 1×10^6 cm^2 s^{-1}. For more details about the VTGCM, see *Brecht et al.* [2011].

2.2. Summary of "Mean" VTGCM Case Results

[13] The results for this study are from a VTGCM "mean" case, which is representative of mean conditions during the VEx sampling period [see *Brecht et al.*, 2011, 2012]. The VEx mean conditions are depicted by statistically averaged

NO and O_2 nightglow emission maps (observed emissions averaged spatially and temporally) [*Gérard et al.*, 2008; *Piccioni et al.*, 2009; *Soret et al.*, 2012]. Specific parameters in the VTGCM are tuned to achieve this "mean" condition, which are given as follows: solar minimum fluxes (F10.7 = 70), the maximum nightside eddy diffusion coefficient (1.0×10^{-7} cm^2 s^{-1}), and the wave drag parameter (0.9×10^{-4} s^{-1}). This "mean" case produced a maximum NO UV nightglow emission near the equator at 108 km. The calculated peak vertical intensity was 2.28 kR (Rayleigh = 10^6 photons cm^{-2} s^{-1} into 4π sr) with a hemispheric average intensity of 0.78 kR. The O_2 IR nightglow emission was also calculated near the equator but at 102 km. The O_2 IR nightglow emission peak vertical intensity, for a three body reaction (O + O + CO_2) yield of 75%, was 2.19 MR with a corresponding hemispheric average intensity of 0.53 MR. The nightglow values are slightly different than previously published in *Brecht et al.* [2011, 2012]. The values differ due to the change in thermal structure (modification of the near-IR heating as described above) and wave drag parameter which was previously 0.5×10^{-4} s^{-1} (modified due to the change in thermal structure). As a result, both nightglow emission peak altitudes increased by 2 km and their peak intensities increased by a factor of ~1.24. The local time or latitude distribution did not change. These nightglow peak intensities for this paper are within the VEx observational ranges and the hemispheric averages agree favorably with the VEx observations [*Brecht et al.*, 2011].

[14] Monitoring and modeling the nightglow emission gives rise to an expanded understanding of the global wind system. Two dominant wind systems are superimposed within the altitude range of ~70 km to ~120 km. The first wind system is a retrograde superrotating zonal (RSZ) flow. It is faster than Venus' rotation and flows in the direction of the planets spin. The second wind system is the subsolar-to-antisolar (SS-AS) flow created by inhomogeneous heating by solar radiation (EUV, UV, and IR) [*Dickinson and Ridley*, 1977; *Schubert et al.*, 1980; *Bougher et al.*, 1997]. The calculated VTGCM neutral zonal winds (combination of the RSZ and SS-AS winds) near the equator at the morning terminator are -108 m s^{-1} at 110 km, -166 m s^{-1} at 120 km, and -150 m s^{-1} near 180 km. The evening terminator winds are 112 m s^{-1} at 110 km, 191 m s^{-1} at 120 km, and 289 m s^{-1} near 180 km. The simulated evening terminator winds are faster than the morning terminator winds because the wave drag term, Rayleigh friction, is prescribed asymmetrically in LT in order to mimic the observed upper atmosphere RSZ winds (see *Brecht et al.* [2011] for details). The prescribed RSZ winds are very weak (<10 m s^{-1}) from ~80 km to 112 km, and above 110 km the emergence of modest RSZ winds approach ~70–80 m s^{-1} above ~130 km. This RSZ profile displays slightly different wind magnitudes than previously presented in *Brecht et al.* [2011], due to the updated VTGCM dayside temperatures. This new RSZ profile is needed to produce the O_2 IR nightglow peak intensity near midnight and to position the NO UV nightglow peak intensity near 01:00 LT.

[15] These simulated VTGCM wind values are within observational ranges [e.g., *Goldstein et al.*, 1991; *Lellouch et al.*, 1994; *Schmülling et al.*, 2000; *Clancy et al.*, 2008; *Sornig et al.*, 2008; *Clancy et al.*, 2012; *Sornig et al.*, 2012]. For example, in an altitude range of 100 km to 105 km,
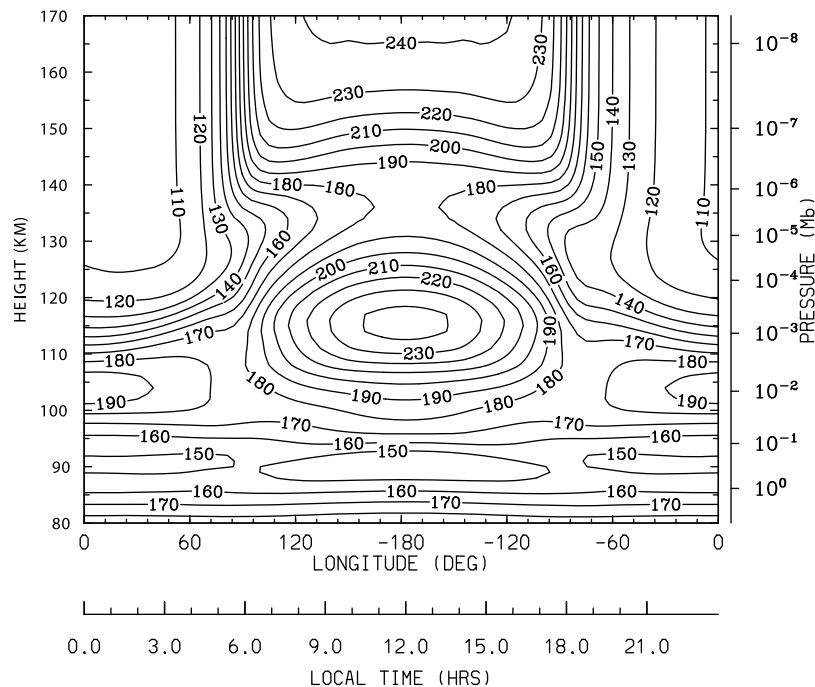
Figure 1. VTGCM temperature (K); longitude-height cross section at 2.5°N (LT vs height).

both observed RSZ and SS-AS winds are highly variable and typically ranging from ~0 to 130 m s^{-1} with an extreme of 300 m s^{-1}. Near 110 km, the general trend shows the RSZ winds to be weak and the SS-AS winds are ~ 120 ±30 m s^{-1}. Above ~120 km the total wind is on average ~200 m s^{-1}. More information about wind measurements can be found in *Lellouch et al.* [1997], *Bougher et al.* [2006], *Clancy et al.* [2012], and *Sornig et al.* [2012].

[16] For more details on the "mean" case, parameters, or observations see *Brecht et al.* [2011] and references within.

3. Results and Discussion for Venus Dayside Upper Atmosphere

[17] The VTGCM reproduces, in concert with observations, characteristics of Venus' upper atmosphere thermal structure. Figure 1 represents the simulated thermal structure near the equator at 2.5°N. On the nightside, the observed warm region at 104 km [e.g., *Bailey et al.*, 2008] is reproduced with a temperature of 198 K. This "mean" warm temperature is largely regulated by the magnitude of the day-to-night SS-AS global circulation and the corresponding downwelling near midnight at the equator [*Brecht et al.*, 2011]. As discussed previously, the 4.3-μm heating on the dayside near 115 km and the corresponding day-to-night global circulation produces a downwelling component on the nightside, which results in dynamical heating near midnight. This "mean" simulation produces a corresponding total dynamical heating rate of 71 K/day at an altitude of 104 km. The simulated nightside warm region is in accord with available VEx and ground based observations [e.g., *Bertaux et al.*, 2007; *Bailey et al.*, 2008]. Above this warm region resides the cold nightside thermosphere (~104 K to

~112 K). At 12:00 LT near 112 km is the dayside warm region, about 244 K, created by near IR (i.e., mostly 4.3-μm) heating. Above the dayside warm region the atmosphere cools initially but eventually warms to ~240 K near the exobase (~190 km) due to solar EUV heating.

[18] Figures 2a and 2b illustrate the corresponding dayside thermal balances near the equator (LT = 12:00 and LT = 16:00). Above 145 km altitude, EUV heating is dominant and is balanced by both molecular conduction and CO_2 15-μm cooling. Below145 km altitude, the near IR heating becomes the dominant heat source which competes with the CO_2 15-μm cooling to control the temperatures. At the lower altitudes (<90 km altitude), adiabatic cooling is stronger than the CO_2 15-μm cooling. Throughout the dayside, total dynamical driven advection (horizontal + vertical) is minimal. These trends of the thermal balances hold true for latitudes of 65°N/S (Figures 2c and 2d), however the magnitudes of the radiative processes decrease and the total dynamical driven advection increases. Therefore, similar to the equator, the radiative processes are most important closer to the polar region near 110 km. Due to the dominance of near IR heating below ~140 km, the solar cycle variations of EUV-UV fluxes would only have a major impact on the thermal balances and temperatures above ~140 km altitude. Therefore, this suggests the warm region on the dayside near 115 km should be persistent throughout the solar cycle and any fluctuations in these temperatures would be directly connected to dynamical fluctuations.

[19] A map of the simulated neutral temperature at 110 km is illustrated in Figure 3. This altitude was chosen to correspond to the ground-based observations made by *Sonnabend et al.* [2010] near 110 km. The warm temperatures at the sub-solar point approach 230 K and decrease to 171 K near
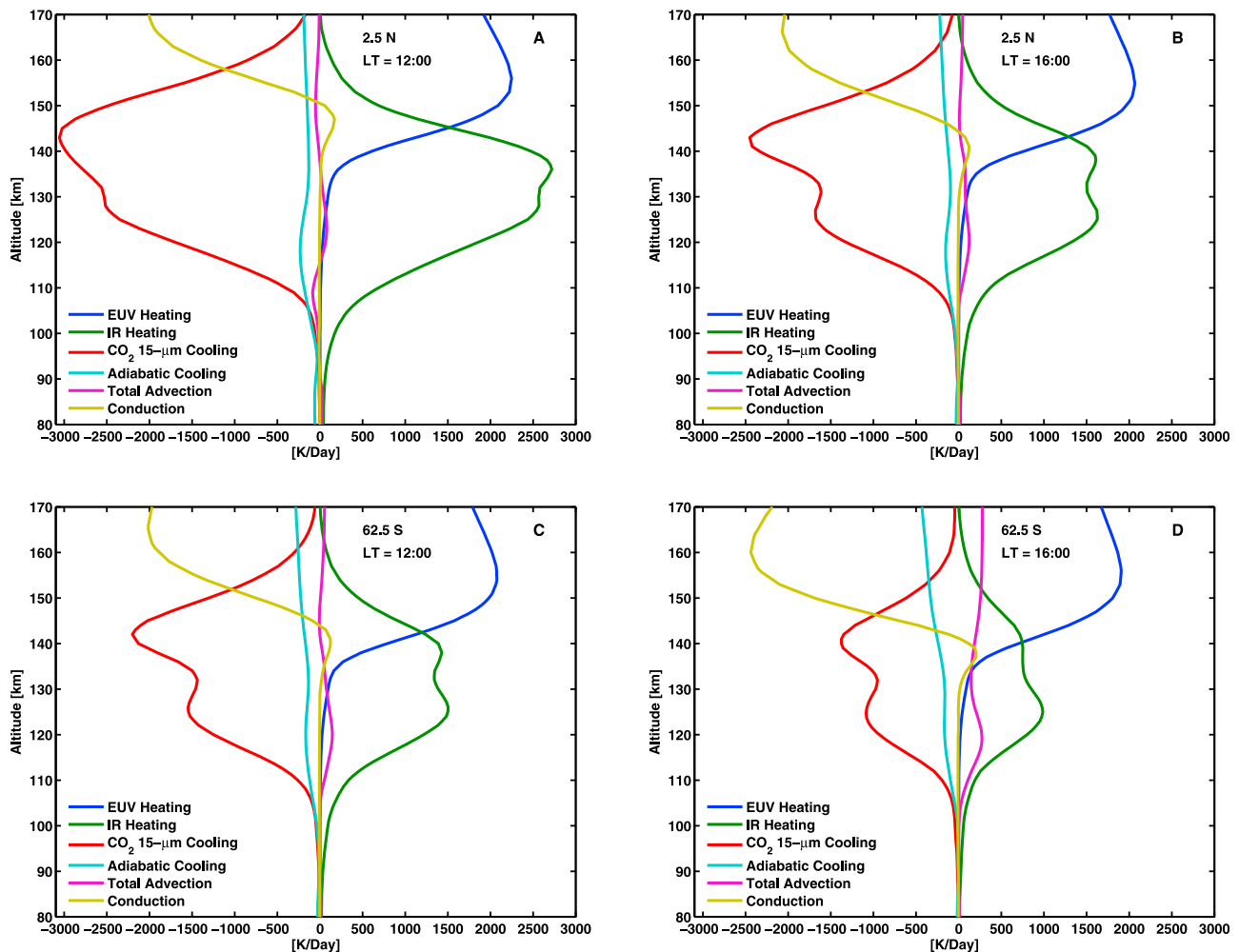
Figure 2. The heating and cooling terms (K/day) at (a) LT = 12:00/Lat. = 2.5 N, (b) LT = 16:00/Lat. = 2.5 N, (c) LT 12:00/Lat. = 62.5 S, and (d) LT = 16:00/Lat. = 62.5 S.

the anti-solar point. Near the poles, the temperatures also decrease to about 170 K to 180 K. Figure 2 in *Sonnabend et al.* [2010] presents a temperature map; however detailed comparisons with this map are very difficult due to the limited coverage and observations. Their peak is near 243 K at 12:00 LT and the equator. Temperatures fall off toward the pole at 12:00 LT, with a minimum temperature of 163 K. The VTGCM simulation has a smaller temperature range compared to these ground based observations; ~230 K at the equator and ~176 K near the pole. Closer to the terminators, the observations suggest smaller temperatures changes from the equator to the poles (~183 K to ~223 K).

[20] Figure 4 shows vertical temperature profiles and the corresponding CO_2 density profiles for selected LT locations near the equator (12:00, 16:00, 18:00). The warm region between 100 km to 115 km is seen at each LT due to the local impact of the 4.3-μm near IR heating rate and the global circulation. This warm region is also reflected in the CO_2 density profiles. As temperatures increase (decrease), scale heights increase (decrease) in the atmosphere. VTGCM temperatures are increasing near 110 km and as a result the CO_2 density scale heights are increasing as well. The VTS3 temperature profile for 12:00 LT, shown in Figure 4 with

"x" symbols, lacks this warm region. The VTS3 temperature near 110 km is ~60 K cooler than the value simulated by the VTGCM. Therefore, the CO_2 density scale height fails to increase in contrast to that visible in the VTGCM simulation. Last, at LT = 18:00, a drop in CO_2 density scale heights over 120 to 135 km is calculated corresponding to cooler local temperatures.

[21] Near 90 km, *Clancy et al.* [2012] sub-millimeter measurements suggest the VTGCM temperatures are ~20 to 50 K colder than observed. The dayside *Clancy et al.* [2012] observations are limited since the main focus of the investigation was upon nightside observations and the Venus disk was too small to obtain good spatial resolution. Nevertheless, these limited observations suggest the VTGCM is missing a heating source in the 80 km to 90 km region. Other measurements by previous missions and ground based observations also suggest this region to be warmer, closer to ~170 K with 20 to 40 K variability [e.g., *Clancy and Muhleman*, 1991]. Radiative transfer models and observations do suggest potential heat sources in this region; aerosol heating in the upper haze layer and the unknown UV absorber are implicated [e.g., *Crisp*, 1986; *Bullock and Grinspoon*, 2001; *Eymet et al.*, 2009]. Neither of those
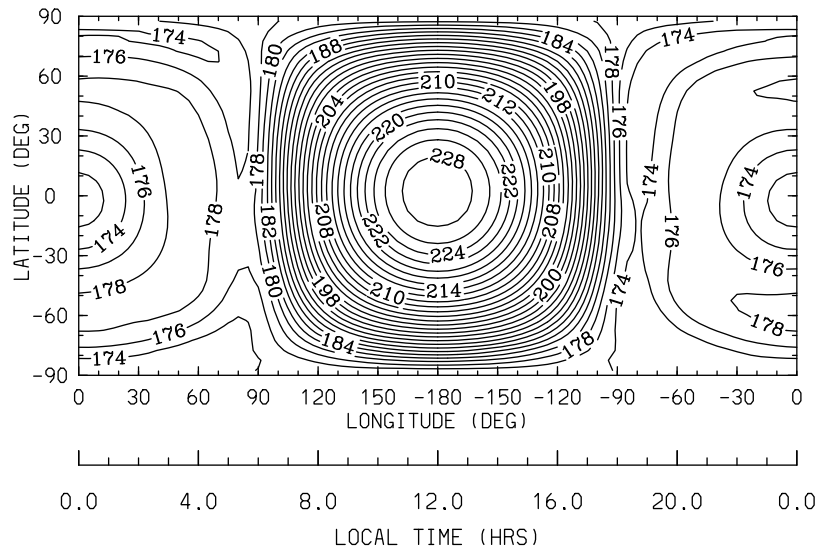
Figure 3. VTGCM temperature (K); altitude slice at 110 km (LT vs latitude). The maximum value is 230 K and the minimum value is 171 K.

sources have been properly addressed in the current VTGCM. Furthermore, latitude variation near 90 km is minimal within the VTGCM results (~10 K change).

[22] A latitudinal representation of VTGCM temperatures is compared with tabulated temperature observations from *Sonnabend et al.* [2010] near 12:00 LT (see Figure 5). The error bar associated with each data point is representative of the range for multiple observations at the specific latitude or if there was only one measurement it is the retrieval error. The observations show a latitudinal trend of the temperatures decreasing toward the poles with an asymmetry, while the VTGCM reproduces this same general trend. Near the poles, the VTGCM is warmer than the observations suggest. Another selected LT with more than one observation by

Sonnabend et al. [2010] is located near 07:00 LT. At this LT, the observed and calculated temperatures decrease toward the poles (figure not shown). However, near the poles (latitude greater than 45°) the measurements are warmer than the calculated temperatures from the VTGCM by ~30 K. This suggests the simulated general circulation is maybe stronger (near the terminators) than that of the real atmosphere during these particular observing periods. Alternatively, the overestimation of heating near the poles could be due to missing localized cooling processes in the model and/or the underestimation of atomic oxygen by the VTGCM [*Brecht et al.*, 2012], which produces an underestimation of the 15-μm cooling. Furthermore, the discrepancy at 07:00 LT could be due to very limited observations.
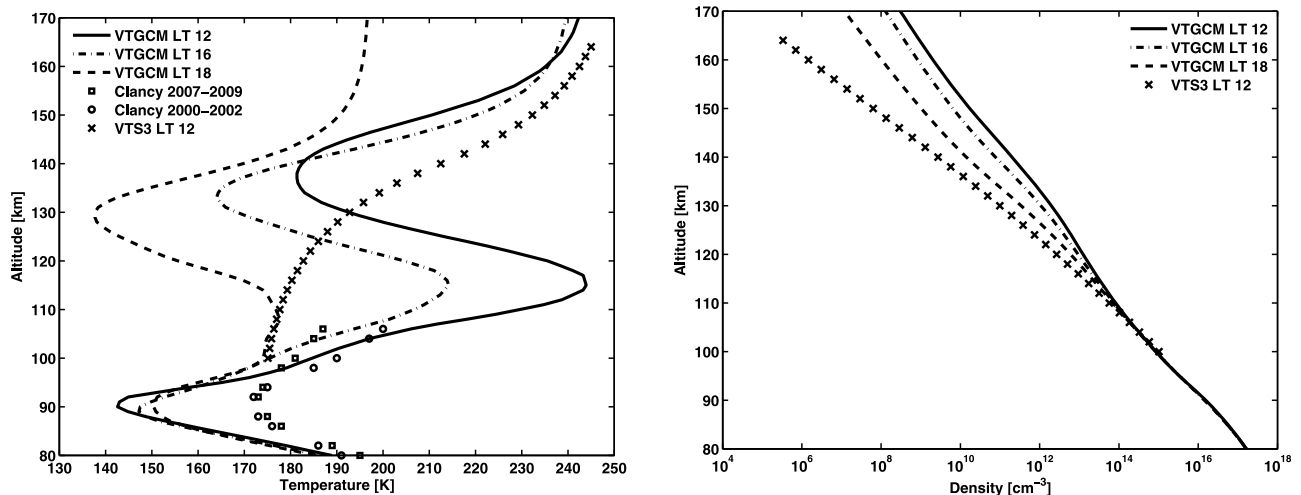

Figure 4. (left) Vertical temperature profiles and (right) CO_2 profiles at 2.5°N for several LT locations. The lined profiles (solid, dashed dot, and dashed) are from VTGCM for 12:00, 16:00, and 18:00 LT, respectively. VTS3 data at 12:00 LT is represented by "x" and is only available above 100 km. For observed temperatures, dayside averaged ground based data from *Clancy et al.* [2012] are represented by the circles and squares. The circles are data during the 2000–2002 observing period, while the squares represent the data from the 2007–2009 observing period.
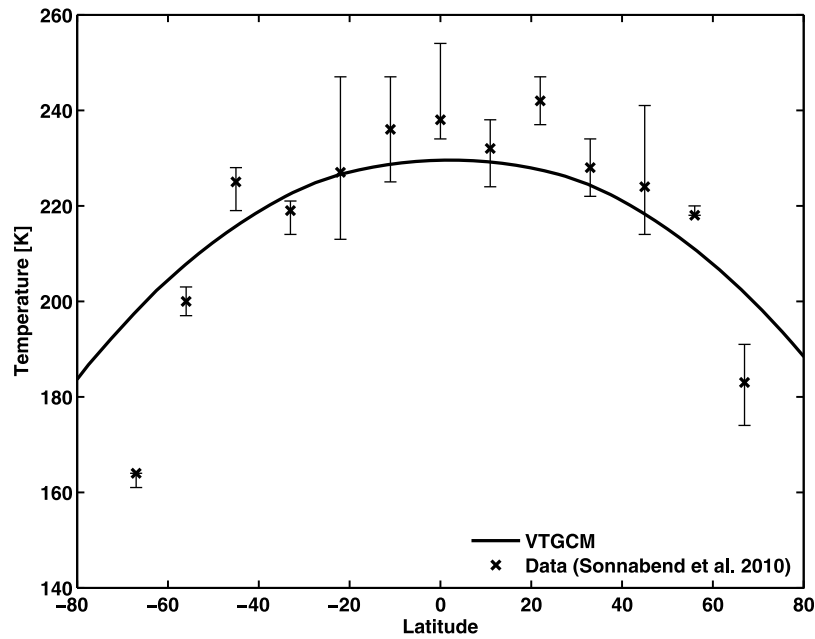
Figure 5. Dayside (12:00 LT) temperatures with respect to latitude for an altitude of 110 km. VTGCM results are the solid line. The "x" represent ground based observations from *Sonnabend et al.* [2010]. The error bars are associated with each data point correspond either (1) to the range for multiple observations at the specific latitude or (2) the retrieval error if there was only one measurement.

However, the simulated temperatures near the equator at 12:00 LT are in close agreement with the observations (240–250 K).

[23] Figure 6 represents the simulated and observed temperature with respect to LT. The observations [*Sonnabend et al.*, 2010] are sparse near the equator at different LT for comparison. However, the VTGCM is ∼5 K colder at LT = 12:00 and the morning terminator values are closer in agreement. The model simulations do not decrease continuously from the sub-solar point to the anti-solar point due to the
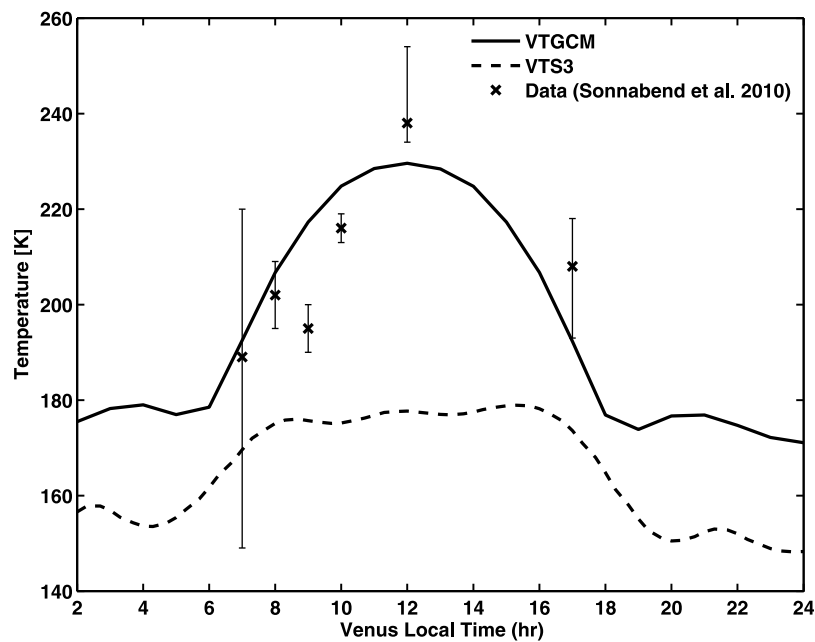

Figure 6. Temperatures with respect to LT at 2.5°N for an altitude of 110 km. VTGCM results are the solid line. The "x" represent ground based observations from *Sonnabend et al.* [2010]. The error bars are associated with each data point correspond either (1) to the range for multiple observations at the specific latitude or (2) the retrieval error if there was only one measurement. VTS3 data is shown as the dashed line.

dynamical heating on the nightside. Furthermore, the warming on the nightside is not symmetrical about the anti-solar point due to the prescribed Rayleigh friction which is used to mimic gravity wave momentum deposition and its impact on the RSZ flow [e.g., *Bougher et al.*, 1988; *Brecht et al.*, 2011]. In addition, VTS3 empirical model temperature data has been included in Figure 6 as the dashed lined. It is clear the VTS3 empirical model poorly represents the warm temperatures near the equator at 12:00 LT. When comparing a constant latitude of 45°S (well observed latitude by *Sonnabend et al.* [2010]), the VTGCM is in best agreement with the measurements near 09:00–10:00 LT (not shown). However, the VTGCM does deviate by ~11 K and ~20 K near 12:00 LT and 07:00 LT respectively. Continuing ground based observations will help characterize the varying temperatures with respect to LT.

4. Conclusion

[24] The VTGCM simulation for solar minimum "mean" conditions, appropriate for recent ground-based (and VEx) sampling, reproduces reasonably well the dayside temperature structure observed near 110 km at noon from 40°S to 40°N latitude. Observed equatorial temperatures spanning dayside LT (07:00 to 17:00) are also well reproduced. However, the VTGCM over-predicts temperatures poleward of 50° latitude. The corresponding low-to-mid latitude heating/cooling rates illustrate a close balance between near-IR heating and CO_2 15-μm cooling near 110 km. This confirms the importance of including the updated near-IR heating and CO_2 15-μm cooling rates presented in *Roldán et al.* [2000] into upper atmosphere GCMs, especially over 100–130 km. Furthermore, the advancement in understanding the processes contributing to non-local thermodynamic equilibrium conditions is important to accurately model the dayside thermal structure of Venus [e.g., *Roldán et al.*, 2000; *López-Valverde et al.*, 2011].

[25] The warm dayside temperature bulge resulting from this radiative balance, centered on 115 ± 5 km, also has implications for the day-to-night thermospheric circulation at this level. Upwelling (divergent) winds near the subsolar point are connected to the downwelling (convergent) winds near the anti-solar point, giving rise to the nightside warm temperature bulge (peaking at 198 K) at ~ 104 ± 5 km. This nightside peak temperature (for mean conditions) is in accord with available spacecraft and ground-based observations collected over many years [e.g., *Bertaux et al.*, 2007; *Bailey et al.*, 2008; *Brecht et al.*, 2011]. The VTGCM suggests that these dayside and nightside lower thermosphere temperature bulges are connected dynamically.

[26] Ongoing spacecraft and ground based observations are needed to fully characterize the dayside thermal structure in the Venus lower thermosphere as a function of LT and latitude. In particular, the time variability of these temperatures, as well as associated winds and composition distributions (e.g., CO_2, CO), needs to be quantified, and climatological averages derived for comparison with GCM model simulations. This approach of combining the structure and wind fields for determining mean conditions, and quantifying the variability about this mean, is crucial for a thorough characterization of the Venus lower thermosphere structure.

[27] It is noteworthy that the VTGCM has been run mostly as a climate model thus far. Upper atmosphere variability can be addressed by adding gravity wave breaking (modifying winds) [e.g., *Zhang et al.*, 1996; *Brecht et al.*, 2011], varying eddy diffusion (adjusting vertical mixing) [*Brecht et al.*, 2011], and/or adding planetary wave forcing (e.g., generating Kelvin waves) [*Hoshino et al.*, 2012]. Our ongoing strategy for data-model comparison studies is proceeding as follows: (a) use the VTGCM "mean" simulations to compare to time and/or spatially averaged datasets, (b) bracket the variability of these datasets about this mean, and (c) adjust the VTGCM tunable parameters (above) to quantify the magnitude of those processes that may drive these observed variations. This is a systematic and effective way to approach data-model studies using a GCM.

[28] In the future, terminator thermal and composition (e.g., CO_2, CO) measurements from the VEx SOIR instrument will be compared in detail with corresponding "mean" VTGCM simulated outputs, extending the current ground-based analysis to recent VEx observations [e.g., *Mahieux et al.*, 2010]. The VTGCM simulation analyzed in this paper can account for average maps of nightside temperatures and airglow intensities and their distributions, in addition to the dayside temperatures presented. The VTGCM also provides terminator temperatures that compare well with previous [*Mahieux et al.*, 2010] and more recent VEx SOIR datasets (A. Mahieux and A.-C. Vandaele, private communication, 2012). Specifically, a preliminary comparison of calculated temperatures in this paper with current VEx SOIR data (A. Mahieux and A.-C. Vandaele, private communication, 2012) shows a remarkable degree of agreement. However, any data analysis study should account for expected differences between the two terminators. PV observations and previous models already suggest there is a noticeable asymmetry in the structure between the morning and eventing terminators [e.g., *Keating et al.*, 1980; *von Zahn et al.*, 1983; *Alexander et al.*, 1993; *Bougher et al.*, 2006], which is the result of the RSZ winds and diurnally variable eddy diffusion. Also, an effective terminator study utilizing the VTGCM will require running at half the horizontal (2.5° × 2.5°) and vertical (0.25 scale height) resolution, in order to resolve the sharp gradients across the terminators more accurately [*Brecht*, 2011].

[29] Finally, the existing VTS3 and VIRA empirical models are inadequate to properly represent the lower thermosphere thermal structure near ~110 km on the dayside. This conclusion has also been found by previous work [e.g., *Bertaux et al.*, 2007; *Pätzold et al.*, 2007; *Drossart et al.*, 2007]. These models are based largely upon PV upper atmosphere measurements obtained mostly at low latitudes above ~140 km. The VTS3 empirical model symmetrically distributes the fields cylindrically at higher latitudes and uses the hydrostatic equilibrium assumption to extrapolate densities below ~140 km. Both the VTS3 and VIRA empirical models should be updated with the recent VEx spacecraft and ground based observations (~100 to 140 km). These updates will provide more valuable empirical model tools to the Venus community that will better characterize the complexity of Venus' upper atmosphere structure and associated dynamics.

References

Alexander, M. J., A. I. F. Stewart, S. C. Solomon, and S. W. Bougher (1993), Local time asymmetries in the Venus thermosphere, *J. Geophys. Res.*, *98*, 10,849–10,871, doi:10.1029/93JE00538.

Bailey, J., S. Chamberlain, D. Crisp, and V. S. Meadows (2008), Near infrared imaging spectroscopy of Venus with the Anglo-Australian Telescope, *Planet. Space Sci.*, *56*, 1385–1390, doi:10.1016/j.pss.2008.03.006.

Bertaux, J.-L., et al. (2007), A warm layer in Venus' cryosphere and high-altitude measurements of HF, HCl, H_2O and HDO, *Nature*, *450*, 646–649, doi:10.1038/nature05974.

Betz, A. L., M. A. Johnson, R. A. McLaren, and E. C. Sutton (1976), Heterodyne detection of CO_2 emission lines and wind velocities in the atmosphere of Venus, *Astrophys. J.*, *208*, L141–L144, doi:10.1086/182251.

Bougher, S. W., and W. J. Borucki (1994), Venus O_2 visible and IR nightglow: Implications for lower thermosphere dynamics and chemistry, *J. Geophys. Res.*, *99*, 3759–3776, doi:10.1029/93JE03431.

Bougher, S. W., R. E. Dickinson, E. C. Ridley, R. G. Roble, A. F. Nagy, and T. E. Cravens (1986), Venus mesosphere and thermosphere: II. Global circulation, temperature, and density variations, *Icarus*, *68*, 284–312, doi:10.1016/0019-1035(86)90025-4.

Bougher, S. W., R. G. E. Roble, R. E. Dickinson, and E. C. Ridley (1988), Venus mesosphere and thermosphere: III. Three-dimensional general circulation with coupled dynamics and composition, *Icarus*, *73*, 545–573, doi:10.1016/0019-1035(88)90064-4.

Bougher, S. W., J.-C. Gérard, A. I. F. Stewart, and C. G. Fesen (1990), The Venus nitric oxide night airglow: Model calculations based on the Venus Thermospheric General Circulation Model, *J. Geophys. Res.*, *95*, 6271–6284, doi:10.1029/JA095iA05p06271.

Bougher, S. W., M. J. Alexander, and H. G. Mayr (1997), Upper atmosphere dynamics: Global circulation and gravity waves, in *Venus II: Geology, Geophysics, Atmosphere, and Solar Wind Environment*, edited by S. W. Bougher, D. M. Hunten, and R. J. Phillips, pp. 259–291, Univ. of Ariz. Press, Tucson.

Bougher, S. W., S. Engel, R. G. Roble, and B. Foster (1999), Comparative terrestrial planet thermospheres: 2. Solar cycle variation of global structure and winds at equinox, *J. Geophys. Res.*, *104*, 16,591–16,611, doi:10.1029/1998JE001019.

Bougher, S. W., R. G. Roble, and T. Fuller-Rowell (2002), Simulations of the upper atmospheres of the terrestrial planets, in *Atmospheres in the Solar System: Comparative Aeronomy*, Geophys. Monogr. Ser. vol. 130, edited by M. Mendillo, A. Nagy, and J. H. Waite, pp. 261–288, AGU, Washington, D. C.

Bougher, S. W., S. Rafkin, and P. Drossart (2006), Dynamics of the Venus upper atmosphere: Outstanding problems and new constraints expected from Venus Express, *Planet. Space Sci.*, *54*, 1371–1380, doi:10.1016/j.pss.2006.04.023.

Bougher, S. W., P. Blelly, M. Combi, J. L. Fox, I. Mueller-Wodarg, A. Ridley, and R. G. Roble (2008), Neutral upper atmosphere and ionosphere modeling, *Space Sci. Rev.*, *139*, 107–141, doi:10.1007/s11214-008-9401-9.

Brecht, A. S. (2011), Tracing the dynamics in Venus' upper atmosphere, PhD thesis, Univ. of Mich., Ann Arbor.

Brecht, A. S., S. W. Bougher, J.-C. Gérard, C. D. Parkinson, S. Rafkin, and B. Foster (2011), Understanding the variability of nightside temperatures, NO UV and O_2 IR nightglow emissions in the Venus upper atmosphere, *J. Geophys. Res.*, *116*, E08004, doi:10.1029/2010JE003770.

Brecht, A., S. Bougher, J.-C. Gérard, and L. Soret (2012), Atomic oxygen distributions in the Venus thermosphere: Comparisons between Venus Express observations and global model simulations, *Icarus*, *217*(2), 759–766, doi:10.1016/j.icarus.2011.06.033.

Bullock, M. A., and D. H. Grinspoon (2001), The recent evolution of climate on venus, *Icarus*, *150*(1), 19–37, doi:10.1006/icar.2000.6570.

Clancy, R. T., and D. O. Muhleman (1991), Long-term (1979–1990) changes in the thermal, dynamical, and compositional structure of the Venus mesosphere as inferred from microwave spectral line observations of ^{12}CO, ^{13}CO, and $C^{18}O$, *Icarus*, *89*, 129–146, doi:10.1016/0019-1035(91)90093-9.

Clancy, R. T., B. J. Sandor, and G. H. Moriarty-Schieven (2003), Observational definition of the Venus mesopause: Vertical structure, diurnal variation, and temporal instability, *Icarus*, *161*, 1–16, doi:10.1016/S0019-1035(02)00022-2.

Clancy, R. T., B. J. Sandor, and G. H. Moriarty-Schieven (2008), Venus upper atmospheric CO, temperature, and winds across the afternoon/evening terminator from June 2007 JCMT sub-millimeter line observations, *Planet. Space Sci.*, *56*, 1344–1354, doi:10.1016/j.pss.2008.05.007.

Clancy, R. T., B. J. Sandor, and G. Moriarty-Schieven (2012), Thermal structure and CO distribution for the Venus mesosphere/lower thermosphere: 2001–2009 inferior conjunction sub-millimeter CO absorption line observations, *Icarus*, *217*(2), 779–793, doi:10.1016/j.icarus.2011.05.032.

Connes, P., J. F. Noxon, W. A. Traub, and N. P. Carleton (1979), $O_2(^1 \Delta)$ emission in the day and night airglow of Venus, *Astrophys. J.*, *233*, L29–L32, doi:10.1086/183070.

Crisp, D. (1986), Radiative forcing of the venus mesosphere: I. Solar fluxes and heating rates, *Icarus*, *67*(3), 484–514, doi:10.1016/0019-1035(86)90126-0.

Crisp, D., V. S. Meadows, B. Bézard, C. de Bergh, J.-P. Maillard, and F. P. Mills (1996), Ground-based near-infrared observations of the Venus nightside: 1.27-μm $O_2(a^1\Delta_g)$ airglow from the upper atmosphere, *J. Geophys. Res.*, *101*, 4577–4594, doi:10.1029/95JE03136.

Dickinson, R. E., and E. C. Ridley (1977), Venus mesosphere and thermosphere temperature structure: II. Day-night variations, *Icarus*, *30*, 163–178, doi:10.1016/0019-1035(77)90130-0.

Drossart, P., et al. (2007), A dynamic upper atmosphere of Venus as revealed by VIRTIS on Venus Express, *Nature*, *450*, 641–645, doi:10.1038/nature06140.

Eymet, V., R. Fournier, J. L. Dufresne, S. Lebonnois, F. Houridn, and M. A. Bullock (2009), Net exchange parameterization of thermal infrared radiative transfer in Venus' atmosphere, *J. Geophys. Res.*, *114*, E11008, doi:10.1029/2008JE003276.

Fox, J. L. (1988), Heating efficiencies in the thermosphere of Venus reconsidered, *Planet. Space Sci.*, *36*, 37–46, doi:10.1016/0032-0633(88)90144-4.

Gérard, J.-C., A. Saglam, G. Piccioni, P. Drossart, C. Cox, S. Erard, R. Hueso, and A. Sánchez-Lavega (2008), Distribution of the O_2 infrared nightglow observed with VIRTIS on board Venus Express, *Geophys. Res. Lett.*, *35*, L02207, doi:10.1029/2007GL032021.

Gilli, G., M. A. López-Valverde, P. Drossart, G. Piccioni, S. Erard, and A. Cardesín Moinelo (2009), Limb observations of CO_2 and CO non-LTE emissions in the Venus atmosphere by VIRTIS/Venus Express, *J. Geophys. Res.*, *114*, E00B29, doi:10.1029/2008JE003112.

Goldstein, J. J., M. J. Mumma, T. Kostiuk, D. Deming, F. Espenak, and D. Zipoy (1991), Absolute wind velocities in the lower thermosphere of Venus using infrared heterodyne spectroscopy, *Icarus*, *94*, 45–63, doi:10.1016/0019-1035(91)90140-O.

Grassi, D., P. Drossart, G. Piccioni, N. I. Ignatiev, L. V. Zasova, A. Adriani, M. L. Moriconi, P. G. J. Irwin, A. Negrão, and A. Migliorini (2008), Retrieval of air temperature profiles in the Venusian mesosphere from VIRTIS-M data: Description and validation of algorithms, *J. Geophys. Res.*, *113*, E00B09, doi:10.1029/2008JE003075. [Printed 114(E9), 2009.]

Grassi, D., A. Migliorini, L. Montabone, S. Lebonnois, A. Cardesin-Moinelo, G. Piccioni, P. Drossart, and L. V. Zasova (2010), Thermal structure of Venusian nighttime mesosphere as observed by VIRTIS-Venus Express, *J. Geophys. Res.*, *115*, E09007, doi:10.1029/2009JE003553.

Hedin, A. E., H. B. Niemann, W. T. Kasprzak, and A. Seiff (1983), Global empirical model of the Venus thermosphere, *J. Geophys. Res.*, *88*, 73–83, doi:10.1029/JA088iA01p00073.

Hoshino, N., H. Fujiwara, M. Takagi, Y. Takahashi, and Y. Kasaba (2012), Characteristics of planetary-scale waves simulated by a new Venusian mesosphere and thermosphere general circulation model, *Icarus*, *217*(2), 818–830, doi:10.1016/j.icarus.2011.06.039.

Keating, G. M., F. W. Taylor, J. Y. Nicholson, and E. W. Hinson (1979a), Short-term cyclic variations and diurnal variations of the Venus upper atmosphere, *Science*, *205*, 62–64, doi:10.1126/science.205.4401.62.

Keating, G. M., R. H. Tolson, and E. W. Hinson (1979b), Venus thermosphere and exosphere: First satellite drag measurements of an extraterrestrial atmosphere, *Science*, *203*, 772–774, doi:10.1126/science.203.4382.772.

Keating, G. M., J. Y. Nicholson, and L. R. Lake (1980), Venus upper atmosphere structure, *J. Geophys. Res.*, *85*, 7941–7956, doi:10.1029/JA085iA13p07941.

Keating, G. M., J.-L. Bertaux, S. W. Bougher, R. E. Dickinson, T. E. Cravens, and A. E. Hedin (1985), Models of Venus neutral upper atmosphere:

Structure and composition, *Adv. Space Res.*, 5, 117–171, doi:10.1016/0273-1177(85)90200-5.

Kliore, A. J., and I. R. Patel (1980), Vertical structure of the atmosphere of Venus from Pioneer Venus orbiter radio occultations, *J. Geophys. Res.*, 85, 7957–7962, doi:10.1029/JA085iA13p07957.

Lee, C., and M. I. Richardson (2010), A general circulation model ensemble study of the atmospheric circulation of Venus, *J. Geophys. Res.*, 115, E04002, doi:10.1029/2009JE003490.

Lee, C., S. R. Lewis, and P. L. Read (2007), Superrotation in a Venus general circulation model, *J. Geophys. Res.*, 112, E04S11, doi:10.1029/2006JE002874.

Lee, C., W. G. Lawson, M. I. Richardson, J. L. Anderson, N. Collins, T. Hoar, and M. Mischna (2011), Demonstration of ensemble data assimilation for Mars using DART, MarsWRF, and radiance observations from MGS TES, *J. Geophys. Res.*, 116, E11011, doi:10.1029/2011JE003815.

Lellouch, E., J. J. Goldstein, J. Rosenqvist, S. W. Bougher, and G. Paubert (1994), Global circulation, thermal structure, and carbon monoxide distribution in Venus' mesosphere in 1991, *Icarus*, 110, 315–339, doi:10.1006/icar.1994.1125.

Lellouch, E., T. Clancy, D. Crisp, A. J. Kliore, D. Titov, and S. W. Bougher (1997), Monitoring of Mesospheric Structure and Dynamics, in *Venus II: Geology, Geophysics, Atmosphere, and Solar Wind Environment*, edited by S. W. Bougher, D. M. Hunten, and R. J. Phillips, pp. 295–324, Univ. of Ariz. Press, Tucson.

López-Valverde, M. A., P. Drossart, R. Carlson, R. Mehlman, and M. Roos-Serote (2007), Non-LTE infrared observations at Venus: From NIMS/Galileo to VIRTIS/Venus Express, *Planet. Space Sci.*, 55, 1757–1771, doi:10.1016/j.pss.2007.01.008.

López-Valverde, M., G. Sonnabend, M. Sornig, and P. Kroetz (2011), Modelling the atmospheric CO_2 10-μm non-thermal emission in Mars and Venus at high spectral resolution, *Planet. Space Sci.*, 59(10), 999–1009, doi:10.1016/j.pss.2010.11.011.

Mahieux, A., A. C. Vandaele, E. Neefs, S. Robert, V. Wilquet, R. Drummond, A. Federova, and J. L. Bertaux (2010), Densities and temperatures in the Venus mesosphere and lower thermosphere retrieved from SOIR on board Venus Express: Retrieval technique, *J. Geophys. Res.*, 115, E12014, doi:10.1029/2010JE003589.

Niemann, H. B., R. E. Hartle, A. E. Hedin, W. T. Kasprzak, N. W. Spencer, D. M. Hunten, and G. R. Carignan (1979), Venus upper atmosphere neutral gas composition: First observations of the diurnal variations, *Science*, 205, 54–56, doi:10.1126/science.205.4401.54.

Niemann, H. B., W. T. Kasprzak, A. E. Hedin, D. M. Hunten, and N. W. Spencer (1980), Mass spectrometric measurements of the neutral gas composition of the thermosphere and exosphere of Venus, *J. Geophys. Res.*, 85, 7817–7827, doi:10.1029/JA085iA13p07817.

Ohtsuki, S., N. Iwagami, H. Sagawa, Y. Kasaba, M. Ueno, and T. Imamura (2005), Ground-based observation of the Venus 1.27-μm O_2 airglow, *Adv. Space Res.*, 36, 2038–2042, doi:10.1016/j.asr.2005.05.078.

Pätzold, M., et al. (2007), The structure of Venus' middle atmosphere and ionosphere, *Nature*, 450, 657–660, doi:10.1038/nature06239.

Piccioni, G., et al. (2009), Near-IR oxygen nightglow observed by VIRTIS in the Venus upper atmosphere, *J. Geophys. Res.*, 114, E00B38, doi:10.1029/2008JE003133.

Rengel, M., P. Hartogh, and C. Jarchow (2008), Mesospheric vertical thermal structure and winds on Venus from HHSMT CO spectral-line observations, *Planet. Space Sci.*, 56, 1368–1384, doi:10.1016/j.pss.2008.07.004.

Roldán, C., M. A. López-Valverde, M. López-Puertas, and D. P. Edwards (2000), Non-LTE infrared emissions of CO_2 in the atmosphere of Venus, *Icarus*, 147, 11–25, doi:10.1006/icar.2000.6432.

Schmülling, F., J. Goldstein, T. Kostiuk, T. Hewagama, and D. Zipoy (2000), High precision wind measurements in the upper Venus atmosphere, *Bull. Am. Astron. Soc.*, 32, 1121.

Schofield, J. T., and F. W. Taylor (1983), Measurements of the mean, solar-fixed temperature and cloud structure of the middle atmosphere of Venus, *Q. J. R. Meteorol. Soc.*, 109, 57–80, doi:10.1256/smsqj.45903.

Schubert, G., et al. (1980), Structure and circulation of the Venus atmosphere, *J. Geophys. Res.*, 85, 8007–8025, doi:10.1029/JA085iA13p08007.

Seiff, A. (1983), Thermal structure of the atmosphere of Venus, in *Venus*, edited by D. M. Hunten, et al., pp. 215–279, Univ. of Ariz. Press, Tucson.

Seiff, A., and D. B. Kirk (1982), Structure of the Venus mesosphere and lower thermosphere from measurements during entry of the Pioneer Venus probes, *Icarus*, 49, 49–70, doi:10.1016/0019-1035(82)90056-2.

Seiff, A., J. T. Schofield, A. J. Kliore, F. W. Taylor, and S. S. Limaye (1985), Models of the structure of the atmosphere of Venus from the surface to 100 kilometers altitude, *Adv. Space Res.*, 5, 3–58, doi:10.1016/0273-1177(85)90197-8.

Sonnabend, G., M. Sornig, R. Schieder, T. Kostiuk, and J. Delgado (2008), Temperatures in Venus upper atmosphere from mid-infrared heterodyne spectroscopy of CO_2 around 10 μm wavelength, *Planet. Space Sci.*, 56, 1407–1413, doi:10.1016/j.pss.2008.05.008.

Sonnabend, G., P. Kroetz, M. Sornig, and D. Stupar (2010), Direct observations of Venus upper mesospheric temperatures from ground based spectroscopy of CO_2, *Geophys. Res. Lett.*, 37, L11102, doi:10.1029/2010GL043335.

Sonnabend, G., et al. (2012), Thermospheric/mesospheric temperatures on Venus: Results from ground-based high-resolution spectroscopy of CO_2 in 1990/1991 and comparison to results from 2009 and between other techniques, *Icarus*, 217(2), 856–862, doi:10.1016/j.icarus.2011.07.015.

Soret, L., J.-C. Gérard, F. Montmessin, G. Piccioni, P. Drossart, and J.-L. Bertaux (2012), Atomic oxygen on the Venus nightside: Global distribution deduced from airglow mapping, *Icarus*, 217(2), 849–855, doi:10.1016/j.icarus.2011.03.034.

Sornig, M., T. Livengood, G. Sonnabend, P. Kroetz, D. Stupar, T. Kostiuk, and R. Schieder (2008), Venus upper atmosphere winds from ground-based heterodyne spectroscopy of CO_2 at 10 μm wavelength, *Planet. Space Sci.*, 56, 1399–1406, doi:10.1016/j.pss.2008.05.006.

Sornig, M., T. Livengood, G. Sonnabend, D. Stupar, and P. Kroetz (2012), Direct wind measurements from November 2007 in Venus' upper atmosphere using ground-based heterodyne spectroscopy of CO_2 at 10 μm wavelength, *Icarus*, 217(2), 863–874, doi:10.1016/j.icarus.2011.03.019.

Taylor, F. W., et al. (1980), Structure and meteorology of the middle atmosphere of Venus Infrared remote sensing from the Pioneer orbiter, *J. Geophys. Res.*, 85, 7963–8006, doi:10.1029/JA085iA13p07963.

von Zahn, U., K. H. Fricke, H. Hoffmann, and K. Pelka (1979), Venus: Eddy coefficients in the thermosphere and the inferred helium content of the lower atmosphere, *Geophys. Res. Lett.*, 6, 337–340.

von Zahn, U., K. H. Fricke, D. M. Hunten, D. Krankowsky, K. Mauersberger, and O. A. Nier (1980), The upper atmosphere of Venus during morning conditions, *J. Geophys. Res.*, 85, 7829–7840, doi:10.1029/JA085iA13p07829.

von Zahn, U., S. Kumar, H. Niemann, and R. Prinn (1983), Composition of the Venus atmosphere, in *Venus*, edited by D. M. Hunten, et al., pp. 299–430, Univ. of Ariz. Press, Tucson.

Zasova, L. V., V. I. Moroz, V. M. Linkin, I. V. Khatuntsev, and B. S. Maiorov (2006), Structure of the Venusian atmosphere from surface up to 100 km, *Cosmic Res.*, 44, 364–383, doi:10.1134/S0010952506040095.

Zhang, S., S. W. Bougher, and M. J. Alexander (1996), The impact of gravity waves on the Venus thermosphere and O_2 IR nightglow, *J. Geophys. Res.*, 101, 23,195–23,206, doi:10.1029/96JE02035.